High-spin terminating states in the N=88 ^{155}Ho and ^{156}Er isotones

J. M. Rees *et al.*

High-spin terminating states in the $N = 88$ ^{155}Ho and ^{156}Er isotones

J. M. Rees,[1] E. S. Paul,[1,*] J. Simpson,[2] M. A. Riley,[3] A. D. Ayangeakaa,[4,†]

M. P. Carpenter,[5] C. J. Chiara,[5,6,‡] U. Garg,[4] P. Hampson,[1] D. J. Hartley,[7]

C. R. Hoffman,[5] R. V. F. Janssens,[5] F. G. Kondev,[8] T. Lauritsen,[5] P. J. R. Mason,[2]

J. Matta,[4] S. L. Miller,[3] P. J. Nolan,[1] J. Ollier,[2] M. Petri,[9,§] D. C. Radford,[10]

J. P. Revill,[1] X. Wang,[3,¶] S. Zhu,[5] J. Gellanki,[11] and I. Ragnarsson[11]

[1]*Oliver Lodge Laboratory, University of Liverpool,*
Liverpool L69 7ZE, United Kingdom

[2]*STFC Daresbury Laboratory, Daresbury,*
Warrington WA4 4AD, United Kingdom

[3]*Department of Physics, Florida State University, Tallahassee, Florida 32306, USA*

[4]*Physics Department, University of Notre Dame, Notre Dame, Indiana 46556, USA*

[5]*Physics Division, Argonne National Laboratory, Argonne, Illinois 60439, USA*

[6]*Department of Chemistry and Biochemistry, College Park,*
University of Maryland, Maryland 20742, USA

[7]*Department of Physics, United States Naval Academy, Annapolis, Maryland 21402, USA*

[8]*Nuclear Engineering Division, Argonne National Laboratory, Argonne, Illinois 60439, USA*

[9]*Nuclear Science Division, Lawrence Berkeley*
National Laboratory, Berkeley, California 94720, USA

[10]*Physics Division, Oak Ridge National Laboratory,*
Oak Ridge, Tennessee 37831, USA

[11]*Division of Mathematical Physics, LTH,*
Lund University, P.O. Box 118, S-22100 Lund, Sweden

(Dated: April 14, 2015)

Abstract

The ^{124}Sn(^{37}Cl,6nγ) fusion-evaporation reaction at a bombarding energy of 180 MeV has been used to significantly extend the excitation level scheme of $^{155}_{67}$Ho$_{88}$. The collective rotational behavior of this nucleus breaks down above spin $I \sim 30$ and a fully aligned non-collective (band terminating) state has been identified at $I^{\pi} = 79/2^{-}$. Comparison with cranked Nilsson-Strutinsky calculations also provides evidence for core-excited non-collective states at $I^{\pi} = 87/2^{-}$ and $(89/2^{+})$ involving particle-hole excitations across the $Z = 64$ shell gap. A similar core-excited state in $^{156}_{68}$Er$_{88}$ at $I^{\pi} = (46^{+})$ is also presented.

PACS numbers: 27.70.+q, 21.10.Re, 23.20.Lv, 23.20.En

*Corresponding author: `esp@ns.ph.liv.ac.uk`

†Present address: Physics Division, Argonne National Laboratory, Argonne, Illinois 60439, USA

‡Present address: U.S. Army Research Laboratory, Adelphi, Maryland 20783, USA

§Present address: Institute für Kernphysik, Technische Universität Darmstadt, D-64289 Darmstadt, Germany

¶Present address: Department of Physics, California Polytechnic State University, San Luis Obispo, California 93407, USA

I. INTRODUCTION

A classic region of band termination at high spin is the one having around ten valence nucleons above the $^{146}_{64}$Gd$_{82}$ closed core [1–7]. At spins around $40 - 50\hbar$ energetically favored non-collective oblate ($\gamma = 60°$) states arise because of the limited number of valence particles available. Above these terminating states, particle-hole excitations of the spherical nuclear core are needed to generate states of higher angular momentum. These core-excited configurations are energetically expensive, characterized by high energy transitions ($\sim 1.0 - 2.5$ MeV) feeding the favored terminating states [8]. These excitations can only increase the available angular momentum by a few units ($\sim 4\hbar$) before terminating in additional non-collective oblate states.

The current work reports many new states in the $^{155}_{67}$Ho$_{88}$ nuclide tracing its shape evolution to high spin. A favored terminating configuration at $I^\pi = 79/2^-$ and subsequent core-excited states at $I^\pi = 87/2^-$ and $(89/2^+)$ have been identified. The experimental states are compared with results from cranked Nilsson-Strutinsky calculations [9–11]. The behavior of ^{155}Ho at high spin is discussed in the context of other $N = 88$ isotones, and in particular ^{156}Er, where a new terminating state at $I^\pi = (46^+)$ has been observed as part of a previous experiment [12–14].

II. EXPERIMENTAL DETAILS

The nucleus ^{155}Ho was studied by γ-ray spectroscopy at the ATLAS accelerator facility of the Argonne National Laboratory, U.S.A., using the Gammasphere γ-ray spectrometer equipped with 101 Compton-suppressed HPGe detectors [15, 16]. A ^{37}Cl beam of energy 180 MeV was used to bombard two stacked thin self-supporting foils of ^{124}Sn, of total thickness 1.1 mg/cm^2, producing ^{155}Ho through the 6n channel. Events were recorded when at least five Compton-suppressed HPGe detectors fired in prompt time coincidence. Over the course of six days of beam time a total of approximately 10^{10} events were recorded. In the off-line analysis, approximately 10^{11} quadruple-coincident γ-ray events (γ^4) were unfolded from the raw data and replayed into a Radware-format four-dimensional hypercube [17, 18] for subsequent analysis. The three most strongly populated nuclei were ^{155}Ho (6n), ^{156}Ho (5n), and ^{157}Ho (4n); in the hypercube they were measured to be populated in a ratio of

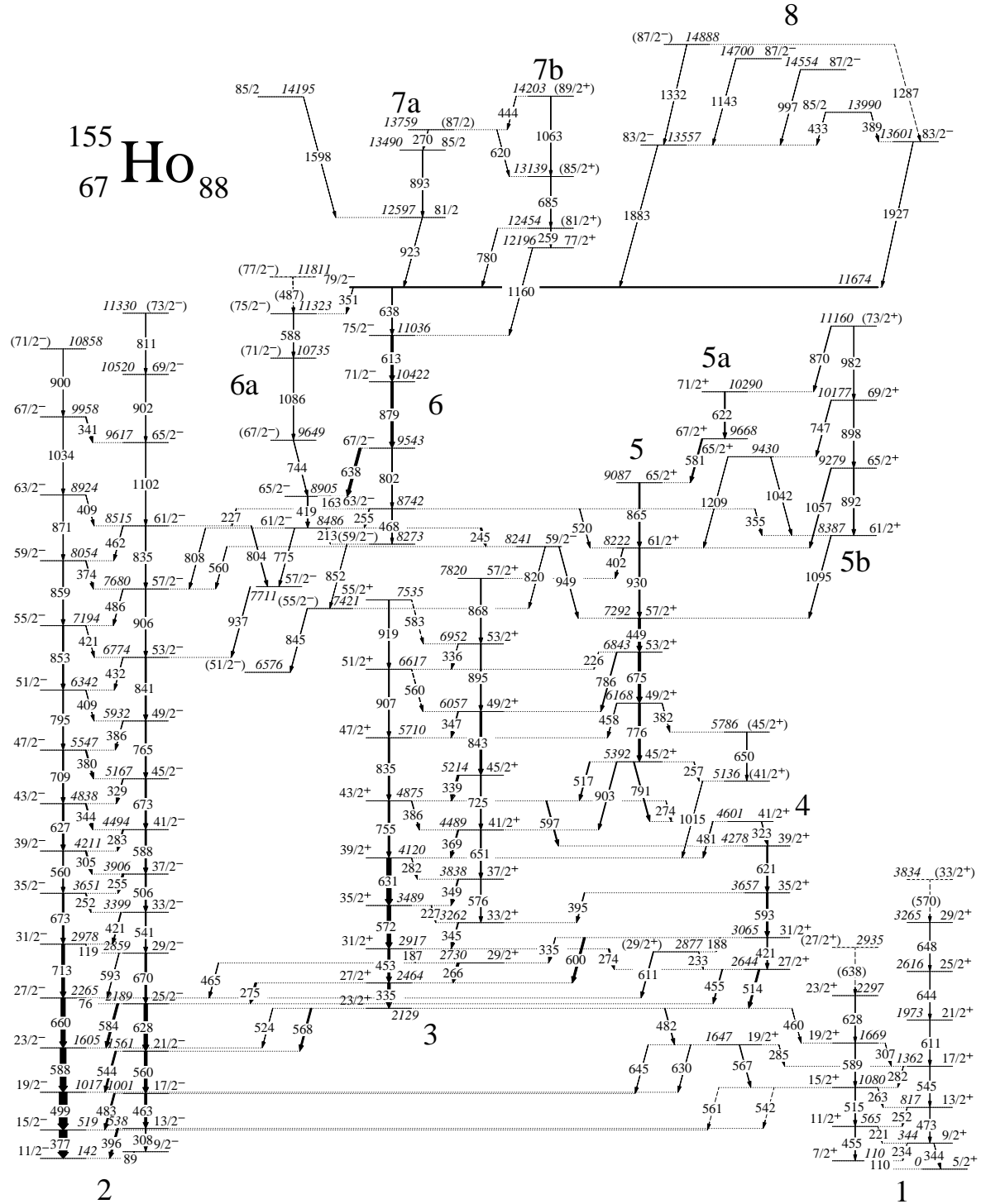FIG. 1: Level scheme deduced for ^{155}Ho. Energies are labeled in keV and the widths of the arrows are proportional to the transition intensities, relative to the 377 keV ($15/2^- \to 11/2^-$) transition (see Table I for additional information).

approximately 0.6:1.0:0.3.

III.   RESULTS

The level scheme deduced for ^{155}Ho is presented in Fig. 1, where structures are labeled 1–8 in order to facilitate the discussion. Some representative coincidence spectra of transitions in ^{155}Ho are shown in Fig. 2. The properties of the γ-ray transitions assigned to ^{155}Ho are listed in Table I. To assist in assigning spins and parities to states in the level scheme, γ-ray multipolarities were extracted from the data by conducting an angular-correlation analysis [19]. Using the technique described in Ref. [20], one-dimensional multiply gated spectra were unfolded from the data that correspond to rings of detectors in Gammasphere at a fixed angle, θ, to the beam direction. It was then possible to evaluate an angular-intensity ratio, defined as

$$R = \frac{I_{\gamma\gamma}[\theta \approx 30°(150°)]}{I_{\gamma\gamma}[\theta \approx 90°]}, \tag{1}$$

for the majority of the transitions. Typically, the angular-intensity ratios extracted from this analysis were ∼0.6 for a pure stretched dipole ($\Delta I = 1$) transition, and ∼1.1 for a stretched quadrupole ($\Delta I = 2$) one.

For the strongly coupled rotational bands 1, 2, and 3, values for the γ decay branching ratio, $\lambda = I_{\gamma}(\Delta I = 1)/I_{\gamma}(\Delta I = 2)$, have been measured for many of the levels. This was achieved by applying double- or triple-gates above the level of interest, producing γ-ray spectra showing the competing dipole and quadrupole transitions depopulating the level. The branching ratios were used to extract $B(M1; I \rightarrow I - 1)/B(E2; I \rightarrow I - 2)$ ratios of reduced transition probabilities. The results are presented in Table II.

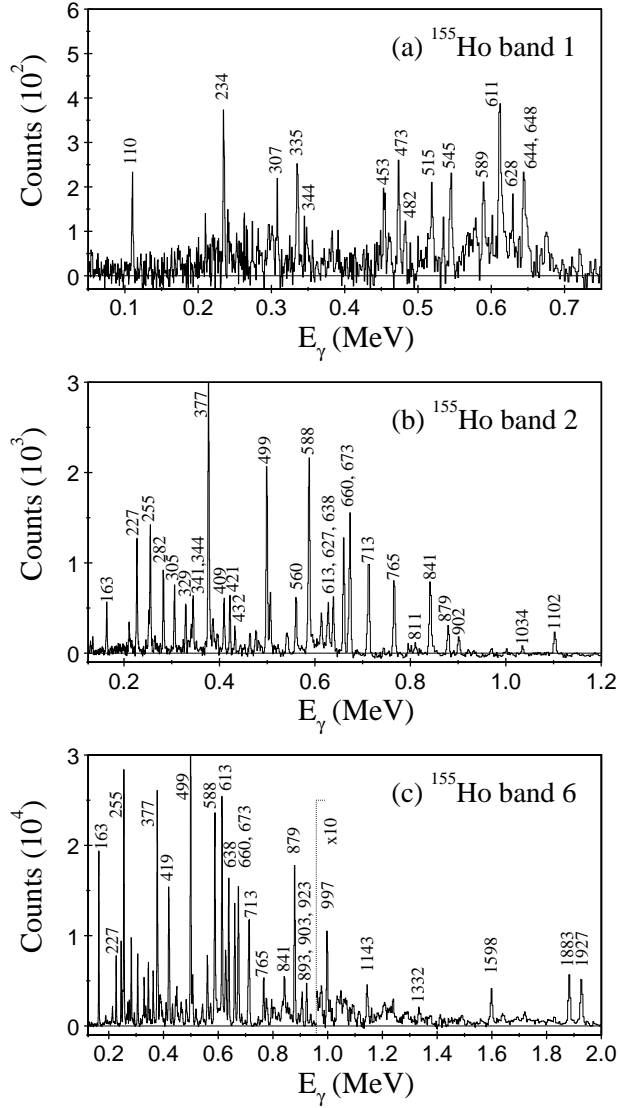FIG. 2: Triple-gated quadruple-coincidence spectra for bands in ^{155}Ho, showing transitions in (a) band 1, (b) band 2, and (c) band 6, labeled by their energies in keV. In (c) the *y*-scale is expanded by a factor of ten above $E_\gamma \sim 0.95$ MeV and the high-energy transitions associated with structure 8 are labeled. In each case, a sum of 'clean' gates was set on each axis of the hypercube.

TABLE I: Energies, intensities, angular-intensity ratios, and spin-parity assignments for the observed ^{155}Ho transitions. The labels used in the final column correspond to those in Fig. 1.

E_γ (keV)[a]	I_γ[b]	R^c	Multipolarity	Assignment	Structure
75.7				$27/2^- \to 25/2^-$	2
88.6	1.8			$9/2^- \to 11/2^-$	2
110.1	9.9	0.53(7)	$M1/E2$	$7/2^+ \to 5/2^+$	1
119.0	3.20			$31/2^- \to 29/2^-$	2
163.4	13.8	0.577(25)	$M1/E2$	$65/2^- \to 63/2^-$	6
187.4	11.6	0.64(5)	$M1/E2$	$31/2^+ \to 29/2^+$	3
187.9	1.18			$31/2^+ \to (29/2^+)$	4
213.0	2.2	0.66(22)	$M1/E2$	$61/2^- \to 59/2^-$	6
220.7				$11/2^+ \to 9/2^+$	1
226.3	2.47			$53/2^+ \to 51/2^+$	$5 \to 3$
226.6	5.61	0.540(21)	$M1/E2$	$63/2^- \to 61/2^-$	$6 \to 2$
227.0	5.3	0.61(5)	$M1/E2$	$35/2^+ \to 33/2^+$	3
233.0	2.7			$(29/2^+) \to 27/2^+$	4
234.0	2.4	0.82(9)	$M1/E2$	$9/2^+ \to 7/2^+$	1
244.8	18.1	0.68(4)	$M1/E2$	$61/2^- \to 59/2^-$	6
251.7	8.6	0.58(3)	$M1/E2$	$35/2^- \to 33/2^-$	2
252.1	1.1	0.94(11)	$M1/E2$	$13/2^+ \to 11/2^+$	1
254.7	20.0	0.585(16)	$M1/E2$	$37/2^- \to 35/2^-$	2
255.4	7.4	0.686(19)	$M1/E2$	$63/2^- \to 61/2^-$	6
256.5	6.1			$45/2^+ \to (41/2^+)$	5
258.7				$(81/2^+) \to 77/2^+$	7b
263.1	1.5			$15/2^+ \to 13/2^+$	1
265.5	25.4	0.62(22)	$M1/E2$	$29/2^+ \to 27/2^+$	3
269.6	2.0	0.91(23)	$(M1/E2)$	$(87/2) \to 85/2$	7a
273.6	16.5			$31/2^+ \to 27/2^+$	$3 \to 4$
274.1	3.1			$43/2^+ \to 41/2^+$	$3 \to 4$
275.3	24.9	0.72(5)	$E1$	$27/2^+ \to 25/2^-$	$3 \to 2$

TABLE I continued.

E_γ (keV)[a]	I_γ[b]	R^c	Multipolarity	Assignment	Structure
281.5				$17/2^+ \to 15/2^+$	1
281.9	5.3	0.79(9)	$M1/E2$	$39/2^+ \to 37/2^+$	3
282.6	12.9	0.63(3)	$M1/E2$	$41/2^- \to 39/2^-$	2
285.3	1.5			$19/2^+ \to 17/2^+$	$3 \to 1$
305.3	13.6	0.70(4)	$M1/E2$	$39/2^- \to 37/2^-$	2
307.3	1.5			$19/2^+ \to 17/2^+$	1
307.6	8.8	1.00(8)	$E2$	$13/2^- \to 9/2^-$	2
323.4	6.9	0.55(9)	$M1/E2$	$41/2^+ \to 39/2^+$	4
329.4	9.1	0.57(6)	$M1/E2$	$45/2^- \to 43/2^-$	2
334.8	6.0	0.78(10)	$M1/E2$	$31/2^+ \to 29/2^+$	$4 \to 3$
335.0	33.2	1.12(9)	$E2$	$27/2^+ \to 23/2^+$	3
335.6	2.7			$53/2^+ \to 51/2^+$	3
339.0	22.7	0.70(9)	$M1/E2$	$45/2^+ \to 43/2^+$	3
340.6	8.3			$67/2^- \to 65/2^-$	2
344.1	12.2	0.66(3)	$M1/E2$	$43/2^- \to 41/2^-$	2
344.1	1.2			$9/2^+ \to 5/2^+$	1
345.2	10.7	0.66(4)	$M1/E2$	$33/2^+ \to 31/2^+$	3
347.4	9.4	0.71(9)	$M1/E2$	$49/2^+ \to 47/2^+$	3
348.8	13.2	0.668(23)	$M1/E2$	$37/2^+ \to 35/2^+$	3
350.7	4.60			$79/2^- \to (75/2^-)$	6
354.9	3.28	0.57(10)	$E1$	$63/2^- \to 61/2^+$	$6 \to 5b$
369.0	14.3	0.622(22)	$M1/E2$	$41/2^+ \to 39/2^+$	3
374.2	7.7			$59/2^- \to 57/2^-$	2
376.7	100	0.983(21)	$E2$	$15/2^- \to 11/2^-$	2
379.5	14.1			$47/2^- \to 45/2^-$	2
381.6	4.7	0.73(9)	$E2$	$49/2^+ \to (45/2^+)$	5
385.8	6.5			$49/2^- \to 47/2^-$	2
386.3	7.1	0.75(11)	$M1/E2$	$43/2^+ \to 41/2^+$	3
388.7	0.7	0.70(10)	$M1/E2$	$85/2 \to 83/2^-$	8

TABLE I continued.

E_γ (keV)[a]	I_γ[b]	R^c	Multipolarity	Assignment	Structure
395.0	8.3	1.04(9)	$M1/E2$	$35/2^+ \to 33/2^+$	$4 \to 3$
396.2	23	0.91(3)	$M1/E2$	$13/2^- \to 11/2^-$	2
401.9	6.3	1.14(5)	$E2$	$61/2^+ \to 57/2^+$	$5 \to 3$
408.9	2.7	0.76(6)	$M1/E2$	$63/2^- \to 61/2^-$	2
409.0	4.7			$51/2^- \to 49/2^-$	2
418.8	12.3	1.04(17)	$E2$	$65/2^- \to 61/2^-$	6
420.5	3.7			$55/2^- \to 53/2^-$	2
420.9	10.9	1.1(3)	$E2$	$31/2^+ \to 27/2^+$	4
421.5	10.3			$33/2^- \to 31/2^-$	2
432.2	4.8	0.69(16)	$M1/E2$	$53/2^- \to 51/2^-$	2
432.8	0.7	0.80(9)	$M1/E2$	$85/2 \to 83/2^-$	8
443.7	1.2	0.84(5)	$(M1/E2)$	$(89/2^+) \to (87/2)$	$7b \to 7a$
448.7	28.4	1.17(3)	$E2$	$57/2^+ \to 53/2^+$	5
453.0	29.2	0.932(9)	$E2$	$31/2^+ \to 27/2^+$	3
454.5	10.6			$27/2^+ \to 25/2^-$	$4 \to 2$
454.7	1.8	1.01(15)	$E2$	$11/2^+ \to 7/2^+$	1
457.9	6.5			$49/2^+ \to 47/2^+$	$5 \to 3$
459.8	4.5	0.94(8)	$E2$	$23/2^+ \to 19/2^+$	$3 \to 1$
461.7	6.6			$61/2^- \to 59/2^-$	2
463.3	29.3	0.970(11)	$E2$	$17/2^- \to 13/2^-$	2
464.5	6.9	0.51(10)	$E1$	$29/2^+ \to 27/2^-$	$3 \to 2$
468.2				$63/2^- \to (59/2^-)$	6
472.8	3.0	1.02(9)	$E2$	$13/2^+ \to 9/2^+$	1
481.0	7.2			$41/2^+ \to 39/2^+$	$4 \to 3$
482.4	8.9	1.10(5)	$E2$	$23/2^+ \to 19/2^+$	3
482.8	19.5			$17/2^- \to 15/2^-$	2
485.6	5.9			$57/2^- \to 55/2^-$	2
487.0				$(77/2^-) \to (75/2^-)$	6a
498.6	100	1.02(3)	$E2$	$19/2^- \to 15/2^-$	2

TABLE I continued.

E_γ (keV)[a]	I_γ[b]	R^c	Multipolarity	Assignment	Structure
506.2	18.0	1.17(7)	$E2$	$37/2^- \to 33/2^-$	2
514.5	21.6			$27/2^+ \to 23/2^+$	$4 \to 3$
515.2	6.0	0.82(17)	$E2$	$15/2^+ \to 11/2^+$	1
516.7	11.1	0.83(19)	$M1/E2$	$45/2^+ \to 43/2^+$	$5 \to 3$
519.8	5.8	0.59(12)	$E1$	$63/2^- \to 61/2^+$	$6 \to 5$
524.1	3.5			$23/2^+ \to 23/2^-$	$3 \to 2$
540.9	14.5			$33/2^- \to 29/2^-$	2
541.7	1.2			$15/2^+ \to 13/2^-$	$1 \to 2$
543.8	20.6			$21/2^- \to 19/2^-$	2
544.6	1.0	1.11(9)	$E2$	$17/2^+ \to 13/2^+$	1
559.6	6.7			$51/2^+ \to 49/2^+$	3
559.6	37.7	1.16(5)	$E2$	$21/2^- \to 17/2^-$	2
559.8	4.9			$59/2^- \to 57/2^-$	$6 \to 2$
559.9	12.3			$39/2^- \to 35/2^-$	2
561.2	1.2			$15/2^+ \to 15/2^-$	$1 \to 2$
566.9	12.4			$19/2^+ \to 15/2^+$	$3 \to 1$
568.1	20.4	0.618(17)	$E1$	$23/2^+ \to 21/2^-$	$3 \to 2$
(569.6)				$(33/2^+) \to 29/2^+$	1
572.3	48.2	1.09(6)	$E2$	$35/2^+ \to 31/2^+$	3
575.8	9.5			$37/2^+ \to 33/2^+$	3
581.1	22.7	0.67(4)	$M1/E2$	$67/2^+ \to 65/2^+$	$5a \to 5$
583.0	23.3			$55/2^+ \to 53/2^+$	3
584.2	26.6	0.72(14)	$M1/E2$	$25/2^- \to 23/2^-$	2
587.9	76.0	1.26(3)	$E2$	$23/2^- \to 19/2^-$	2
587.9	19.6	1.13(3)	$E2$	$41/2^- \to 37/2^-$	2
588.0	3.0			$(75/2^-) \to (71/2^-)$	6a
589.4	4.5			$19/2^+ \to 15/2^+$	1
592.9	23.8			$35/2^+ \to 31/2^+$	4
593.3	6.0			$29/2^- \to 27/2^-$	2

TABLE I continued.

E_γ (keV)^a	I_γ ^{b}	R^c	Multipolarity	Assignment	Structure
596.9	13.7			$43/2^+ \to 39/2^+$	$3 \to 4$
600.3	26.2			$31/2^+ \to 27/2^+$	$4 \to 3$
611.1	3.6	1.23(6)	$E2$	$21/2^+ \to 17/2^+$	1
611.5	9.0			$(29/2^+) \to 27/2^-$	$4 \to 2$
613.5	33.6	1.25(7)	$E2$	$75/2^- \to 71/2^-$	6
620.0				$(87/2^+) \to (85/2^+)$	$7a \to 7b$
620.9	15.6			$39/2^+ \to 35/2^+$	4
622.4	12.3	1.53(13)	$E2$	$71/2^+ \to 67/2^+$	5a
626.7	21.0	1.19(6)	$E2$	$43/2^- \to 39/2^-$	2
627.7	6.0	1.19(6)	$E2$	$23/2^+ \to 19/2^+$	1
628.1	46.0	1.2(7)	$E2$	$25/2^- \to 21/2^-$	2
629.5	4.5			$19/2^+ \to 19/2^-$	$3 \to 2$
630.6	58.6	1.20(5)	$E2$	$39/2^+ \to 35/2^+$	3
638.1	32.0	0.51(3)	$M1/E2$	$67/2^- \to 65/2^-$	6
638.3	18.0	1.10(7)	$E2$	$79/2^- \to 75/2^-$	6
(638.4)	9.1			$(27/2^+) \to 23/2^+$	1
643.8	1.5			$25/2^+ \to 21/2^+$	1
645.3	4.1			$19/2^+ \to 17/2^-$	$3 \to 2$
648.1				$29/2^+ \to 25/2^+$	1
650.0				$(45/2^+) \to (41/2^+)$	5
650.9	13.5	1.60(23)	$E2$	$41/2^+ \to 37/2^+$	3
660.1	55.9	1.15(4)	$E2$	$27/2^- \to 23/2^-$	2
669.7	23.5			$29/2^- \to 25/2^-$	2
673.2	21.8	1.21(3)	$E2$	$35/2^- \to 31/2^-$	2
673.4	19.9			$45/2^- \to 41/2^-$	2
675.4	34.7	1.13(8)	$E2$	$53/2^+ \to 49/2^+$	5
684.8	2.2	1.17(11)	$E2$	$(85/2^+) \to (81/2^+)$	7b
708.9	15.4	0.98(11)	$E2$	$47/2^- \to 43/2^-$	2
712.5	38.2	1.14(4)	$E2$	$31/2^- \to 27/2^-$	2

TABLE I continued.

E_γ (keV)^a	$I_\gamma{}^b$	R^c	Multipolarity	Assignment	Structure
725.3	13.0	1.07(5)	$E2$	$45/2^+ \to 41/2^+$	3
743.7	6.0	0.70(10)	$(M1/E2)$	$(67/2^-) \to 65/2^-$	6a $\to$ 6
746.8	6.9	1.08(15)	$E2$	$69/2^+ \to 65/2^+$	5b $\to$ 5a
755.3	22.3	1.23(19)	$E2$	$43/2^+ \to 39/2^+$	3
765.3	17.2	1.12(5)	$E2$	$49/2^- \to 45/2^-$	2
775.2	5.7	1.18(18)	$E2$	$61/2^- \to 57/2^-$	6a
776.1	26.2	0.99(7)	$E2$	$49/2^+ \to 45/2^+$	5
779.7	3.0			$(81/2^+) \to 79/2^-$	7b $\to$ 6
785.9	10.6	1.07(15)	$E2$	$53/2^+ \to 49/2^+$	5 $\to$ 3
791.2	12.4	1.15(16)	$E2$	$45/2^+ \to 41/2^+$	5 $\to$ 4
794.9	12.2	0.91(9)	$E2$	$51/2^- \to 47/2^-$	2
801.8	5.4	1.07(16)	$E2$	$67/2^- \to 63/2^-$	6
804.3	8.2			$61/2^- \to 57/2^-$	2 $\to$ 6
807.6	4.5			$61/2^- \to 57/2^-$	6 $\to$ 2
810.8	5.3			$(73/2^-) \to 69/2^-$	2
820.0	3.0			$59/2^- \to (55/2^-)$	6
834.7	20.0	0.85(5)	$E2$	$47/2^+ \to 43/2^+$	3
835.2	10.0	0.75(7)	$E2$	$61/2^- \to 57/2^-$	2
841.3	18.1	0.92(4)	$E2$	$53/2^- \to 49/2^-$	2
842.8	26.1	0.93(17)	$E2$	$49/2^+ \to 45/2^+$	3
845.0	3.0			$(55/2^-) \to (51/2^-)$	6
851.5				$(59/2^-) \to (55/2^-)$	6
852.7	16.0	1.10(11)	$E2$	$55/2^- \to 51/2^-$	2
859.2	11.1	1.03(15)	$E2$	$59/2^- \to 55/2^-$	2
864.9	18.0	1.18(11)	$E2$	$65/2^+ \to 61/2^+$	5
867.7	11.3	0.99(22)	$E2$	$57/2^+ \to 53/2^+$	3
869.7	6.5			$(73/2^+) \to 71/2^+$	5b $\to$ 5a
870.7	7.0			$63/2^- \to 59/2^-$	2
879.1	31.3	1.18(10)	$E2$	$71/2^- \to 67/2^-$	6

TABLE I continued.

E_γ (keV)[a]	I_γ[b]	R^c	Multipolarity	Assignment	Structure
892.5	10.8	1.03(23)	$E2$	$65/2^+ \to 61/2^+$	5b
892.7	6.2	1.02(5)	$E2$	$85/2 \to 81/2$	7a
895.1	12.9	1.11(18)	$E2$	$53/2^+ \to 49/2^+$	3
898.4	7.8	0.88(10)	$E2$	$69/2^+ \to 65/2^+$	5b
900.1	4.3			$(71/2^-) \to 67/2^-$	2
902.1	3.7	1.19(12)	$E2$	$69/2^- \to 65/2^-$	2
902.9	9.8	1.22(13)	$E2$	$45/2^+ \to 41/2^+$	$5 \to 3$
906.5	10.1	1.10(8)	$E2$	$57/2^- \to 53/2^-$	2
906.9	12.1	0.95(17)	$E2$	$51/2^+ \to 47/2^+$	3
918.5	11.6	1.5(4)	$E2$	$55/2^+ \to 51/2^+$	3
922.9	7.2	0.75(9)	$\Delta I = 1$	$81/2 \to 79/2^-$	$7a \to 6$
930.1	18.5	1.13(8)	$E2$	$61/2^+ \to 57/2^+$	5
937.1	6.5	1.44(24)	$E2$	$57/2^- \to 53/2^-$	$6 \to 2$
948.8	6.1	0.51(9)	$E1$	$59/2^- \to 57/2^+$	$6 \to 5$
982.2	3.4			$(73/2^+) \to 69/2^+$	5b
997.4	1.5	0.92(14)	$E2$	$87/2^- \to 83/2^-$	8
1015.4	2.0	0.51(4)	$M1/E2$	$(41/2^+) \to 39/2^+$	5
1033.9	5.8	1.5(3)	$E2$	$67/2^- \to 63/2^-$	2
1042.4	3.9			$65/2^+ \to 61/2^+$	$5a \to 5b$
1057.1	8.8	0.97(3)	$E2$	$65/2^+ \to 61/2^+$	$5b \to 5$
1063.4	0.1			$(89/2^+) \to (85/2^+)$	7b
1086.2	5.0	1.28(16)	$E2$	$(71/2^-) \to (67/2^-)$	6a
1095.1	6.2	1.16(4)	$E2$	$61/2^+ \to 57/2^+$	$5b \to 5$
1102.2	2.9	1.4(5)	$E2$	$65/2^- \to 61/2^-$	2
1142.9	0.8	1.6(4)	$E2$	$87/2^- \to 83/2^-$	8
1159.6	0.7	0.72(9)	$E1$	$77/2^+ \to 75/2^-$	$7b \to 6$
1208.8	3.5	1.20(12)	$E2$	$65/2^+ \to 61/2^+$	$5a \to 5$
1287.5				$(87/2^-) \to 83/2^-$	8
1331.5				$(87/2^-) \to 83/2^-$	8

TABLE I continued.

E_γ (keV)[a]	I_γ[b]	R^c	Multipolarity	Assignment	Structure
1598.3	1.6	1.00(12)	$E2$	$85/2 \to 81/2$	$\to 7a$
1882.6	2.5	1.23(9)	$E2$	$83/2^- \to 79/2^-$	$8 \to 6$
1926.6	2.3	1.12(8)	$E2$	$83/2^- \to 79/2^-$	$8 \to 6$

[a]The γ-ray energies are estimated to be accurate to ± 0.3 keV.

[b]Intensities quoted as a percentage of the 377-keV ($15/2^- \to 11/2^-$) transition. Errors are estimated to be less than 5% of the quoted values for strong transitions ($I_\gamma > 10$) and less than 10% of the quoted values for the weaker transitions. Intensities for the weakest transitions ($I_\gamma \ll 1$) are not given.

[c]Angular-intensity ratios, R. Pure stretched-dipole transitions typically have $R \approx 0.6$, while stretched-quadrupole ones have $R \approx 1.1$.

A.   New states in ^{155}Ho, bands 1-5

Bands 1–3 consist of strongly coupled structures comprising interleaved signature partners of stretched-$E2$ transitions linked by $\Delta I = 1$ dipole transitions. In the positive-parity band 1, which decays to the $I^\pi = 5/2^+$ ground state, both the $7/2^+$ and $9/2^+$ levels at 110 keV and 344 keV have been previously reported [21]. With the exception of the placement of a 473-keV transition, their ordering is corroborated by this work, and the band is now firmly established up to $23/2^+$ and $29/2^+$, respectively, for the two signatures, or tentatively $(27/2^+)$ and $(33/2^+)$. The 472.5-keV transition reported by Foin $et\ al.$ [22] was thought to feed the $7/2^+$ state, suggesting the existence of an $11/2^+$ state at 503 keV, linked to the $9/2^+$ level via a 238 keV transition. The energy is consistent with that of an observed 472.8-keV transition in this work. However, no 238-keV γ ray has been found associated with this structure, and coincidence relations show that the 473-keV transition feeds the $9/2^+$ state. Its angular-intensity ratio is typical of stretched-$E2$ radiation. The levels in band 1 are higher in energy than those in band 2 of similar spin, and are, hence, more weakly populated.

Previous decay studies of ^{155}Er have shown a 31.8-keV $M2$ transition in ^{155}Ho linking the $11/2^-$ band-head of band 2 with the $7/2^+$ state of band 1 [21]. While it is not possible to observe this transition in the current experiment, new transitions linking band 1 with band 3 and, by extension, the rest of the level scheme, show that the separation in energy between the $11/2^-$ and $7/2^+$ states is 31.9 keV, consistent with Ref. [21].

At low spin, band 2 is the most strongly populated structure in ^{155}Ho. The two signature partners representing this band were previously observed up to $I^\pi = 59/2^-$ and $61/2^-$ [23], and have now been extended up to states at $I^\pi = (71/2^-)$ and $(73/2^-)$. Band 2 is a rotational band consisting of both $\alpha = -1/2$ and $\alpha = +1/2$ signature components, though below $\sim 17\hbar$ the $\alpha = -1/2$ component lies significantly lower in energy. Due to the large staggering between the signature components, some of the interlinking $\Delta I = 1$ transitions were too low in energy to be observed. The multipolarities of many of the transitions have been confirmed, along with the coincidence relations and subsequent ordering of the transitions.

The structure labeled band 3 was previously observed up to $I^\pi = 47/2^+$ and $49/2^+$ [23]. It decays to band 2 via four γ rays, three of which have angular-intensity ratios

TABLE II: Experimental $B(M1; I \rightarrow I - 1)/B(E2; I \rightarrow I - 2)$ ratios of reduced transition probabilities in ^{155}Ho.

I^π	$E_\gamma(I \rightarrow I - 1)$ (keV)	$E_\gamma(I \rightarrow I - 2)$ (keV)	Branching ratio λ $I_\gamma(M1)/I_\gamma(E2)$	$B(M1)/B(E2)$ $(\mu_N/eb)^2$
		band 1		
$9/2^+$	234	344	2.1(3)	0.71(8)
$11/2^+$	221	455	0.45(6)	0.56(7)
$13/2^+$	252	473	0.27(3)	0.28(3)
$15/2^+$	263	515	0.25(5)	0.35(7)
$17/2^+$	282	545	0.38(7)	0.57(10)
$19/2^+$	307	589	0.29(3)	0.49(5)
		band 2		
$13/2^-$	396	308	6.6(15)	0.20(4)
$17/2^-$	483	463	0.88(7)	0.116(9)
$21/2^-$	544	560	0.59(7)	0.142(18)
$25/2^-$	584	628	0.32(5)	0.109(16)
$27/2^-$	76	588	0.0067(6)	0.76(7)
$29/2^-$	593	670	0.36(4)	0.162(18)
$31/2^-$	119	713	0.0149(11)	1.14(8)
$33/2^-$	421	541	1.29(22)	0.56(9)
$35/2^-$	252	673	0.24(3)	1.45(17)
$37/2^-$	305	560	0.65(6)	0.88(9)
$47/2^-$	380	709	0.56(9)	1.28(19)
$49/2^-$	386	765	0.28(3)	0.90(9)
$51/2^-$	409	795	0.25(5)	0.80(16)
$53/2^-$	432	841	0.238(25)	0.87(9)
$55/2^-$	421	853	0.69(25)	2.3(7)
$57/2^-$	486	906	0.260(25)	0.97(9)
$61/2^-$	462	835	0.33(7)	0.95(21)
$63/2^-$	409	871	0.69(5)	3.5(3)

TABLE II continued.

I^π	$E_\gamma(I \to I-1)$	$E_\gamma(I \to I-2)$	Branching ratio λ	$B(M1)/B(E2)$
	(keV)	(keV)	$I_\gamma(M1)/I_\gamma(E2)$	$(\mu_N/eb)^2$
		band 3		
$31/2^+$	187	453	0.110(9)	0.224(19)
$35/2^+$	227	572	0.040(5)	0.146(19)
$37/2^+$	349	576	4.6(8)	4.9(9)
$39/2^+$	282	631	0.086(8)	0.274(24)
$41/2^+$	369	651	1.64(16)	2.7(3)
$43/2^+$	386	755	0.103(7)	0.308(22)
$45/2^+$	339	725	1.42(16)	5.1(6)
$49/2^+$	347	843	0.37(4)	2.6(3)

typical of $\Delta I = 1$ dipole transitions. The absence of any stretched-quadrupole linking transition suggests that those observed are electric dipole ($E1$) in character, and that this structure, therefore, has positive parity. Moreover, it decays to the positive-parity band 1 via stretched-quadrupole transitions, confirming this positive-parity assignment. Band 3 is observed between $23/2^+$ and $57/2^+$ and is yrast between $31/2^+$ and $39/2^+$. It is fed by decays from band 5. A short cascade of stretched-$E2$ transitions is observed in Fig. 1 between spins $39/2^+$ and $27/2^+$, and has been labeled band 4. Fed by decays from bands 3 and 5, it also decays to band 3, as well as band 2. The band has signature $\alpha = -1/2$. A level, tentatively assigned spin-parity $(29/2^+)$, at 2877 keV, and linked by $\Delta I = 1$ transitions to the $27/2^+$ and $31/2^+$ states, may belong to the signature partner of band 4.

An irregular positive-parity structure, band 5, that is briefly yrast at spins $57/2^+$ and $61/2^+$ is also observed, and mainly decays to levels in band 3. The decays to the positive-parity band 3 include stretched-$E2$ transitions, which indicates that band 5 also has positive parity. Above $61/2^+$ and $65/2^+$, band 5 is fed by two short sequences labeled band 5a and 5b in Fig. 1.

B.   New levels in ^{155}Ho at high spin: bands 6–8

Some of the transitions in band 6 have been seen previously, though not linked to the rest of the level scheme [23]. Band 6 decays, in a rather fragmented manner, to $\alpha = +1/2$ levels in band 2 between spins 53/2 and 61/2, and also to band 5. By extracting angular-correlation information for the more strongly populated γ rays in the band, it has been possible to assign spin values up to the 79/2$^-$ state. The presence of a 638-keV doublet in band 6 made it neccessary to take care when selecting coincidence gates for the angular-correlation measurements. It was possible to extract an angular-intensity ratio of 1.10(7) for the higher-spin 638-keV transition, demonstrating that it is most likely of stretched-$E2$ character. The measured ratio for the more intense 67/2$^-$ $\rightarrow$ 65/2$^-$ 638-keV transition was 0.51(3), consistent with a stretched-dipole radiation.

A cascade of γ rays, labeled 6a, decays parallel to band 6. It has not been possible to directly measure the spins of levels in 6a, and there is some ambiguity over the ordering of the 744- and 1086-keV lines. The angular-intensity ratio measured for the 744-keV transition is indicative of stretched-dipole nature. This implies that the 1086-, 588-, and 351-keV transitions must then all be stretched-$E2$ ones to connect to the 79/2$^-$ state of band 6.

There are two further structures, labeled 7a and 7b, which lie higher in energy than the 79/2$^-$ state. The structure labeled 7a consists of 270- and 893-keV transitions, and 7b consists of a cascade of three γ rays of energies 259, 685, and 1063 keV. The two are linked by two γ rays of energies 444 and 620 keV. Due to their weak population, it has not been possible to extract angular-intensity ratios for enough transitions to firmly establish the spins and parities of all the levels up to the highest excitation. The proposed, tentative, assignments are consistent with these data where possible, and are informed by the theoretical calculations presented in Section IV B, which predict favored positive-parity terminating structures above $40\hbar$. The angular-intensity ratios that have been measured are consistent with a change in parity in the decay from 7a and 7b to band 6; both the 923- and 1160-keV transitions have ratios typical of a stretched-$E1$ ($I \rightarrow I - 1$) transition.

A set of levels at the highest excitation energies is labeled 8 in Fig. 1. Notable are the two high-energy (1883- and 1927-keV) transitions feeding the 79/2$^-$ level, Fig. 2(c). With angular-intensity ratios typical of stretched-$E2$ transitions, these indicate the presence of two high-lying 83/2$^-$ states. The 83/2$^-$ level at 13.557 MeV is in turn fed by four γ rays.
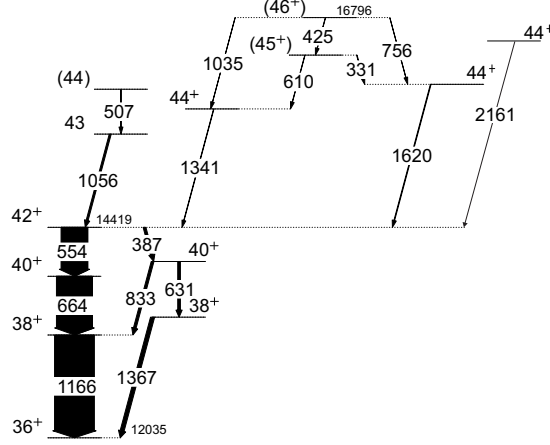
FIG. 3: High-spin level scheme deduced for ^{156}Er [12]. Energies are labeled in keV and the widths of the arrows are proportional to the transition intensities.

Angular-correlation analysis indicates that the 433-keV γ ray is of dipole character, whereas the 997- and 1143-keV transitions are stretched-$E2$ transitions. Thus, the highest-spin negative-parity levels reported in this work have spin 87/2, and lie at 14.554 and 14.700 MeV. The 433-keV line indicates the presence of an $I = 85/2$ state, confirmed by the observation of a 389-keV dipole transition decaying to the other $83/2^-$ level. The 1332-keV transition proved to be too weakly populated to reliably extract angular-correlation information, and, as such, the level at 14.888 MeV is labeled $(87/2^-)$.

C. New levels in ^{156}Er at high spin

New transitions at high spin have been recently observed in the nucleus ^{156}Er [12] as part of a previous experiment, again using the Gammasphere spectrometer. Excited states in ^{156}Er were populated via the ^{114}Cd(^{48}Ca,6nγ) reaction [13, 14]. A partial level scheme showing the high-spin levels in ^{156}Er, including a favored 42^+ terminating state and the excitations above it, is found in Fig. 3. Four previously unreported transitions at high spin have been observed with energies 331, 425, 756, and 1035 keV. The 331-keV transition supports the previous observation of a (45^+) state 1952 keV above the 42^+ terminating state. Seen in coincidence with the 331-, 610-, 1341-, and 1620-keV transitions, there is a γ ray of energy 425 keV, indicating that there exists a further level at 2377 keV above the 42^+ state, labeled (46^+) at an excitation energy of 16.796 MeV. Spectra illustrating some of the
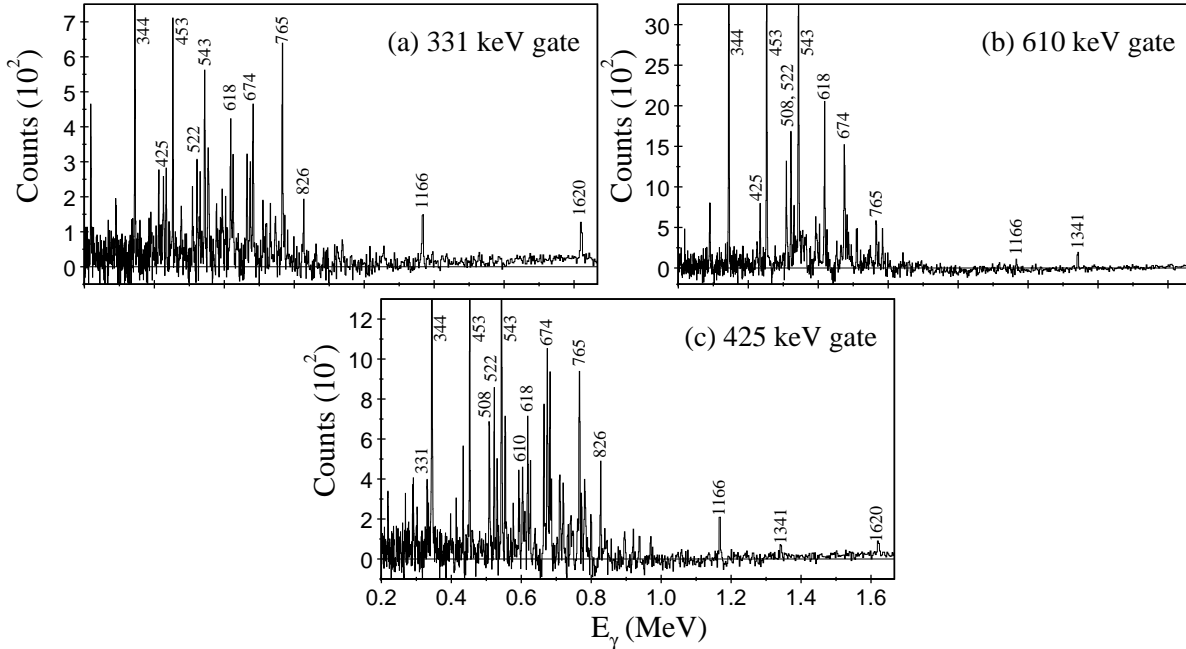
FIG. 4: Triple-gated quadruple-coincidence spectra for ^{156}Er. In all three cases, a list of transitions in bands 1 and 3 has been used as the gating condition on two axes of the hypercube. On the third axis, a gate has been set at (a) 331 keV, (b) 610 keV, and (c) 425 keV. The 331-keV γ ray is coincident with 1620 keV, the 610-keV γ ray with 1341 keV, and 425 keV is seen in coincidence with both. In each spectrum, the transitions are labeled by their energies in keV.

coincidence relationships in ^{156}Er at high spin are provided in Fig. 4. The presence of the (46^+) level is confirmed through the observation of two γ rays of energy 1035 and 756 keV, which are seen in coincidence with the 1341- and 1620-keV γ rays, respectively.

The newly observed γ rays are very weakly populated, with maximum intensities $\sim 1\%$ of the 554-keV $42^+ \rightarrow 40^+$ transition in ^{156}Er, which itself only carries around 2% of the intensity of the $2^+ \rightarrow 0^+$ transition. The intensities of transitions observed in ^{156}Er above the 42^+ state are given in Table III. Although these were too weak to perform an angular-correlation analysis, the decay of the new state into two 44^+ states, directly and via the (45^+) level, is consistent with a tentative spin-parity assignment of $I^\pi = (46^+)$.

IV. DISCUSSION

Rare-earth nuclei with a limited number of neutrons above the $N = 82$ shell closure, and protons above $Z = 64$, lie in a transitional region where collective behavior varies rapidly

TABLE III: Transitions in ^{156}Er above the 42^+ terminating state. Intensities are normalized to the 554-keV $(42^+ \to 40^+)$ transition $(\equiv 100\%)$.

E_γ (keV)	$I_i^\pi \to I_f^\pi$			Relative Intensity (%)
331	(45^+)	$\to$	44^+	1.70(13)
425	(46^+)	$\to$	(45^+)	< 1
507	(44)	$\to$	43	3.6(3)
610	(45^+)	$\to$	44^+	< 1
756	(46^+)	$\to$	44^+	< 1
1035	(46^+)	$\to$	44^+	< 1
1056	43	$\to$	42^+	7.2(5)
1341	44^+	$\to$	42^+	1.38(12)
1620	44^+	$\to$	42^+	2.45(22)
2161	44^+	$\to$	42^+	< 1

with changing particle number at low spin [24, 25]. They tend to be susceptible to shape changes in the triaxial γ plane; i.e., they are γ soft. As they are rotated to high spin the nuclear shape evolves and they exhibit energetically favored non-collective high-spin band-terminating states at around $40 - 50\hbar$ dependent on the limited number of valence particles available outside the ^{146}Gd closed core [1].

For a prolate shape in $^{155}_{67}$Ho$_{88}$, the $N = 88$ Fermi level lies below the first $N_{\mathrm{osc}} = 6$ $(\nu i_{13/2})$ intruder orbital and above the first three $N_{\mathrm{osc}} = 5$ $(\nu f_{7/2}/h_{9/2})$ orbitals. For an oblate shape, the $N = 88$ Fermi level lies above the first $\nu f_{7/2}$, $\nu h_{9/2}$, and $\nu i_{13/2}$ orbitals. The relevant orbitals near the $Z = 67$ Fermi surface arise from states in the middle of the $N_{\mathrm{osc}} = 5$ subshell $(\pi h_{11/2})$ and from the states at the top of the $N_{\mathrm{osc}} = 4$ subshell $(\pi d_{5/2}/g_{7/2}$ and $d_{3/2})$. Where it becomes neccessary to discuss structures in terms of their quasiparticle configurations, the labeling convention set out in Table IV will be used.

The structures in ^{155}Ho are collective up to spin $\sim 30\hbar$. In order to investigate the rotational properties of the bands, the experimental alignments [26],

$$i_{\mathrm{x}}(\omega) = I_{\mathrm{x}}(\omega) - I_{\mathrm{x,ref}}(\omega), \qquad (2)$$

are plotted in Fig. 5 as a function of rotational frequency, $\omega = \Delta E/\Delta I_x \approx E_\gamma/2\hbar$. At a

TABLE IV: Quasiparticle labeling scheme for ^{155}Ho.

Label	$(\pi, \alpha)_n$	Main shell model component at $\hbar\omega = 0$
	Quasineutrons	
A	$(+, +1/2)_1$	$i_{13/2}$
B	$(+, -1/2)_1$	$i_{13/2}$
E	$(-, +1/2)_1$	$f_{7/2}/h_{9/2}$
F	$(-, -1/2)_1$	$f_{7/2}/h_{9/2}$
	Quasiprotons	
A_p	$(-, -1/2)_1$	$h_{11/2}$
B_p	$(-, +1/2)_1$	$h_{11/2}$
C_p	$(-, -1/2)_2$	$h_{11/2}$
D_p	$(-, +1/2)_2$	$h_{11/2}$
E_p	$(+, -1/2)_1$	$N_{\text{osc}} = 4$
F_p	$(+, +1/2)_1$	$N_{\text{osc}} = 4$

given spin I, the aligned spin is $I_{\text{x}} = \sqrt{I(I+1) - K^2}$, while the rotational reference, $I_{\text{x,ref}}$, is given by

$$I_{\text{x,ref}}(\omega) = \omega(\mathcal{J}_0 + \mathcal{J}_1\omega^2). \tag{3}$$

Harris parameters [27] $\mathcal{J}_0 = 32.1 \ \hbar^2\text{MeV}^{-1}$ and $\mathcal{J}_1 = 34.0 \ \hbar^4\text{MeV}^{-3}$, used for ^{157}Ho in Ref. [28], have been adopted here as well. The energies of the bands are given, relative to a rigid-rotation reference [9], in Fig. 6.

For the rotational bands 1, 2, and 3, which include levels of both $\alpha = -1/2$ and $\alpha = +1/2$ signature, experimental $B(M1)/B(E2)$ cascade-to-crossover transition strength ratios have been calculated from the measured branching ratios, $\lambda = I_\gamma(\Delta I = 1)/I_\gamma(\Delta I = 2)$. The $B(M1; I \to I-1)/B(E2; I \to I-2)$ ratio of reduced transition probabilities was determined as:

$$\frac{B(M1)}{B(E2)} = \frac{\lambda}{1.43} \frac{[E_\gamma(\Delta I = 2)]^5}{[E_\gamma(\Delta I = 1)]^3} \ (\mu_N/eb)^2, \tag{4}$$

with γ-ray energies in MeV. The $\Delta I = 1$ transitions were assumed to be pure stretched-dipole in character, with an $E2/M1$ multipole mixing ratio $\delta \equiv 0$. Whilst for nonzero δ, Eq. 4
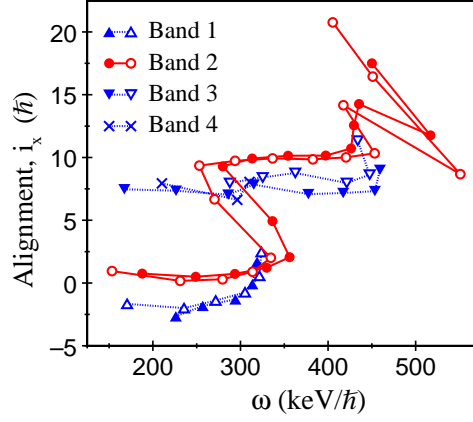
FIG. 5: (Color online) Experimental alignments, i_x, as a function of rotational frequency, ω, for bands 1–4. The open and closed symbols represent the two signature components of the respective bands.
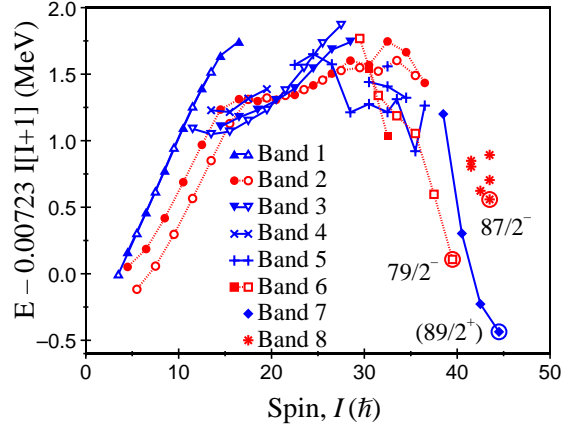

FIG. 6: (Color online) Level energies in ^{155}Ho, plotted as a function of spin, relative to a rigid-rotation reference [9]. Candidate band-terminating states are labeled.

should be modified by a factor of $(1+\delta^2)^{-1}$, the effect this has is small since, typically, $\delta^2 \ll 1$. Indeed, the errors introduced by the experimental branching ratios λ are significantly larger than the effect of neglecting δ. The extracted $B(M1)/B(E2)$ ratios are included in Table II and plotted in Fig. 7. Also presented in Fig. 7 are $B(M1)/B(E2)$ calculations made using the geometric model of Dönau and Frauendorf [29, 30] for the proposed configuration of each structure. Pure single-particle g factors were used in these calculations and the rotational g factor taken as Z/A.
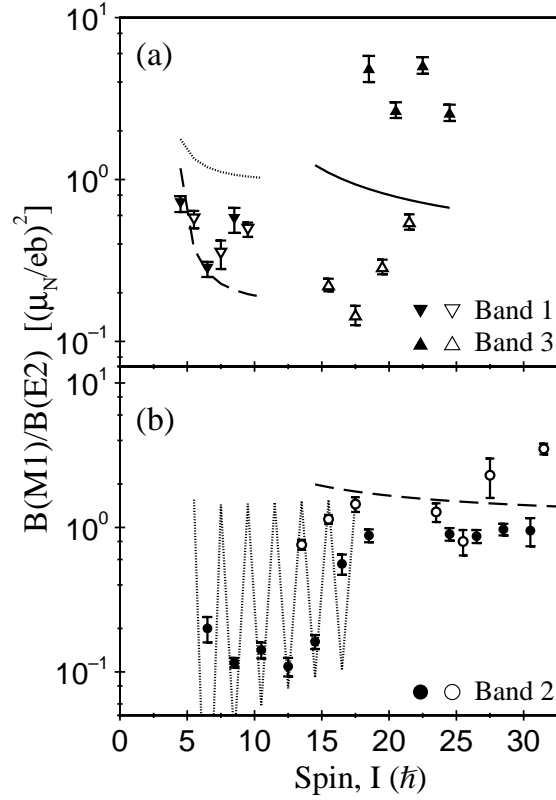
FIG. 7: Values of $B(M1; I \to I-1)/B(E2; I \to I-2)$, calculated from measured γ-ray branching ratios for (a) positive-parity bands 1 and 3, and (b) the negative-parity band 2. The results are listed in Table II. The lines show the results of calculations using the geometrical model of Refs. [29, 30]. In plot (a), calculations have been made for the $[402]5/2^+$ $\pi d_{5/2}$ orbital (dotted line), the $[404]7/2^+$ $g_{7/2}$ orbital (dashed), and the $A_p AE$ quasiparticle configuration (solid). In plot (b), the calculations are made for the $[523]7/2^-$ $\pi h_{11/2}$ orbital (dotted line) including a signature-splitting term, and for the same orbital plus an $i_{13/2}$ neutron alignment, this time with no signature splitting term.

The staggering parameter, $S(I)$ [33], defined as

$$S(I) = E(I) - E(I-1) - 1/2[E(I+1)$$
$$-E(I) + E(I-1) - E(I-2)], \tag{5}$$

is plotted for the rotational bands 1-3 in Fig. 8. The staggering parameter characterizes the degree of 'signature splitting' between the energies of the $\alpha = 1/2$ and $\alpha = -1/2$ signature components of a band.
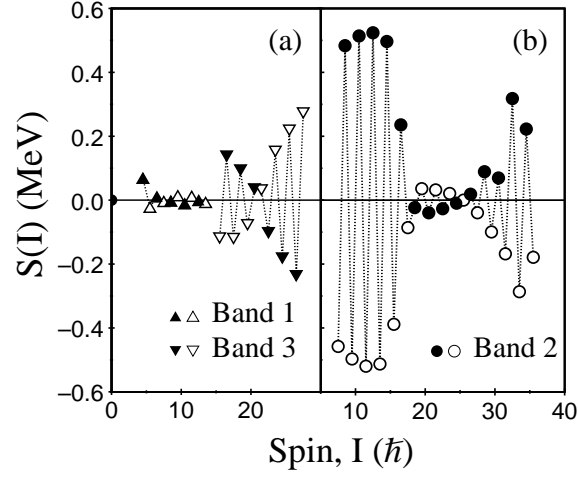
FIG. 8: Staggering parameter $S(I)$ as a function of spin I for (a) positive-parity bands 1 and 3, and (b) negative-parity band 2 in ^{155}Ho.

TABLE V: Proposed quasiparticle configurations of rotational bands in ^{155}Ho.

Band	(π, α)	Configuration
1	$(+, -1/2)$	$E_{\rm p}$
	$(+, +1/2)$	$F_{\rm p}$
2	$(-, -1/2)$	$A_{\rm p} \rightarrow A_{\rm p}AB \rightarrow A_{\rm p}B_{\rm p}C_{\rm p}AB$
	$(-, +1/2)$	$B_{\rm p} \rightarrow B_{\rm p}AB \rightarrow A_{\rm p}B_{\rm p}D_{\rm p}AB$
3	$(+, +1/2)$	$A_{\rm p}AE$
	$(+, -1/2)$	$B_{\rm p}AE$
4	$(+, -1/2)$	$A_{\rm p}AF$

A. Rotational structures: bands 1-4

Specific configurations are proposed for the rotational bands 1–4 based on their alignment properties and their relative energies. These are given in Table V in terms of the single-quasiparticle configurations listed in Table IV.

1. Band 1

The $I^\pi = 5/2^+$ ground state of ^{155}Ho is associated with the [402]5/2$^+$ proton orbital at the top of the $\pi d_{5/2}$ subshell [31]. As such, band 1 may be interpreted as a rotational sequence built on the [402]5/2$^+$ proton configuration, with the 7/2$^+$ level located at 110 keV representing the first rotational state. However, Foin *et al.* [22] proposed that this level represents the [404]7/2$^+$ intrinsic state of the $\pi g_{7/2}$ subshell, decaying to the ground state via the 110-keV transition. The measured $B(M1)/B(E2)$ ratios for band 1, which are plotted alongside calculations for the two orbitals in Fig. 7, appear to support this interpretation, the values being in better agreement with the calculations for a $g_{7/2}$ proton than those for a $d_{5/2}$ one.

In Fig. 5 it can be seen that at $\omega \approx 0.3$ MeV/$\hbar$, band 1 experiences the beginnings of an upbend or backbend. This corresponds to the frequency expected for the alignment of two $i_{13/2}$ neutrons (AB).

2. Band 2

Band 2 is built on the $\pi h_{11/2}$ orbital [523]7/2$^-$ [22]. In Fig. 5, it can be seen that band 2 experiences a backbend at $\omega \approx 0.3$ MeV/$\hbar$, resulting in a gain in alignment of $\sim 10\hbar$. This is understood in terms of a rotational alignment of a pair of $i_{13/2}$ neutrons, AB. In the nomenclature of Table IV, band 2 has an A_p and B_p quasiparticle configuration below the backbend for its $\alpha = -1/2$ and $\alpha = +1/2$ signature components, respectively. Above the backbend, its quasiparticle configuration is $A_\mathrm{p}AB$ and $B_\mathrm{p}AB$, respectively.

Figure 5 suggests what may be a second alignment corresponding to an upbend at $\omega \approx 0.45$ MeV/$\hbar$. Since the A_p (B_p) quasiproton is already present in the $\alpha = -1/2$ ($\alpha = +1/2$) signature of band 2, the alignment of the first pair of $h_{11/2}$ protons ($A_\mathrm{p}B_\mathrm{p}$) is blocked. The next allowed crossings involve the next two $\pi(h_{11/2})^2$ protons, the $B_\mathrm{p}C_\mathrm{p}$ orbitals for the $\alpha = -1/2$ levels, and $A_\mathrm{p}D_\mathrm{p}$ orbitals for the $\alpha = +1/2$ levels. Cranked Woods-Saxon calculations show that both crossings are expected to occur at a frequency of approximately 0.4 MeV/$\hbar$. It was proposed in Ref. [32] that similar upturns in aligned angular momentum at the top of the $\pi h_{11/2}$ band of ^{157}Ho correspond to such $B_\mathrm{p}C_\mathrm{p}$ and $A_\mathrm{p}D_\mathrm{p}$ crossings.

Due to the low energy of the $\alpha = -1/2 \rightarrow \alpha = +1/2$ transitions, it has only been possible

to measure the $B(M1)/B(E2)$ ratios of the highest of the $\alpha = -1/2$ levels, $27/2^-$, $31/2^-$ and $35/2^-$, before the AB backbend. Even so, the measured $B(M1)/B(E2)$ ratios exhibit a strong signature dependence which disappears in levels above the backbend. Calculations with the geometric model of Dönau and Frauendorf reproduce signature dependence of this kind when a signature splitting term ($\pm \Delta e'/\hbar\omega$ [29, 30]) is introduced. Indeed, a notable feature of band 2 is the large signature splitting it exhibits at low spin, of order 0.25 MeV, which disappears above the backbend at around spin 35/2. The calculations of Fig. 7 have been made for the $[523]7/2^-$ $\pi h_{11/2}$ orbital including a signature-splitting term, and for the same orbital plus an $i_{13/2}$ neutron alignment, this time without a signature splitting term.

While band 1 exhibits little staggering, $S(I)$, in Fig. 8, there is a large one observed in band 2, which disappears at $I \approx 15$ at the first $i_{13/2}$ neutron alignment. At the highest spins in band 2, the staggering returns, perhaps reflecting a further change in its structure. In the $\pi h_{11/2}$ band of ^{157}Ho, a similar return of signature splitting is observed at spin $\sim 28\hbar$. This similarity in behavior supports the view that ^{155}Ho experiences the same $B_p C_p$ and $A_p D_p$ crossings at the top of band 2 that have been reported in ^{157}Ho [32]. Though not to the same extent as band 2, band 3 exhibits some signature splitting, with an inversion occuring at $I \approx 21$, below which the $\alpha = -1/2$ signature component is favored.

Previously, it has been argued that the large staggering in band 2 is evidence for triaxiality in ^{155}Ho at low spin [34, 35]. Cranked shell-model calculations suggest that for a configuration built on a single $h_{11/2}$ proton an energy minimum exists for a negative-γ, axially asymmetric shape, with significant splitting between the A_p and B_p configurations. Coupling the $h_{11/2}$ proton to the AB, $i_{13/2}$ neutron alignment ($A_p AB$ and $B_p AB$) has the effect of quenching both the γ deformation and the signature splitting. This is in accord with the large staggering observed at the bottom of band 2, but not above the backbend.

Signature splitting and γ deformation are not predicted for the $\pi d_{5/2}/g_{7/2}$ configuration and, for the $\pi h_{11/2}$ plus $\nu i_{13/2} h_{11/2}$ configuration ($A_p AE$ and $B_p AE$) corresponding to band 3, there is quenching of both the signature splitting and γ deformation. In this light, the signature splitting observed in ^{155}Ho can be seen as indirect evidence of triaxiality at low spin, driven by the $\pi h_{11/2}$ orbital. A complex picture emerges of the shape evolution of ^{155}Ho, in which competing triaxial and prolate shapes coexist at low spin, built on $\pi h_{11/2}$ and $\pi d_{5/2}/g_{7/2}$ protons respectively, with a triaxial-prolate transition occuring in band 2 at the $\nu i_{13/2}$ alignment.

3. Band 3

The positive-parity band 3 passes through the AB crossing region without experiencing any increase in aligned angular momentum, see Fig. 5, which suggests that the AB crossing is blocked and its quasiparticle configuration already involves an $i_{13/2}$ neutron. Its alignment of $\sim 8\hbar$ more than the band 2 $\pi h_{11/2}$ configuration is consistent with a $\pi(h_{11/2}) \otimes \nu(i_{13/2}f_{7/2}/h_{9/2})$ $A_{\mathrm{p}}(B_{\mathrm{p}})AE$ three-quasiparticle assignment. Similar three-quasiparticle structures are common in the mass $A = 130$ region where the neutron Fermi surface is near $N = 70$; e.g., Ref. [36], as opposed to the proton Fermi surface near $Z = 70$ here. Strangely, the measured $B(M1)/B(E2)$ values in band 3, see Fig. 7, show a striking signature dependence; the $\alpha = -1/2$ levels are strongly populated from $\alpha = +1/2$ decays, but the decays in the opposite direction are few in comparison. By introducing a signature splitting term to the $A_{\mathrm{p}}AE$ geometric-model calculations, such signature dependence can be reproduced, but the splitting must be approximately 0.2 MeV in magnitude, with $\alpha = +1/2$ being the favored signature. In reality, while some splitting is observed, it is much smaller (less than 0.1 MeV) and there is a reversal in the favored signature at $I \approx 21$, below which $\alpha = -1/2$ is favored. Cranked shell-model calculations put this three-quasiparticle configuration at the lowest energy, lower in fact than the $A_{\mathrm{p}}AB$ configuration, which agrees with the fact that the band is yrast at spins 31/2 to 39/2, and makes other interpretations of its structure unlikely. The effects of triaxiality on the signature dependence of $B(M1)/B(E2)$ ratios has been discussed in Ref. [37].

4. Band 4

Band 4 has $\alpha = -1/2$ and has a similar alignment to band 3, see Fig. 5. When the energies of band 4 are plotted as a function of spin in Fig. 6, it can be seen that it is higher in energy than band 3, lying at a similar energy to band 2 at the AB neutron crossing. The $A_{\mathrm{p}}AF$ three-quasiparticle configuration is predicted to be at a higher energy than the $A_{\mathrm{p}}AE$ one, and to be competitive with the $A_{\mathrm{p}}AB$ configuration. Relative to the $h_{11/2}[523]7/2^{-}$ proton, the $A_{\mathrm{p}}AF$ configurations would be expected to have a gain in alignment similar to that of the $A_{\mathrm{p}}AE$ one, which agrees with what is seen in Fig. 5. It is, therefore, proposed that band 4 corresponds to the $A_{\mathrm{p}}AF$ three-quasiparticle configuration.

B.   High-spin behavior: Cranked Nilsson-Strutinsky calculations

In order to interpret the high-spin behavior of ^{155}Ho, theoretical calculations have been performed in the framework of the configuration-dependent cranked Nilsson-Strutinsky (CNS) formalism [9, 10]. For the κ and μ Nilsson model parameters, which define the $\mathbf{l{\cdot}s}$ and $\mathbf{l^2}$ strengths of the modified oscillator potential, respectively, the $A = 150$ parameters of Ref. [38] have been adopted. The calculations do not take into account the effect of pairing and, as a result, can only be considered realistic at relatively high spin ($I \gtrsim 30$). In the results presented here, absolute energies at high spin are calculated [11] based on the Lublin-Strasbourg drop (LSD) model [39] and a rigid moment of inertia calculated with a radius parameter $r_0 = 1.16$ fm and a diffuse surface [40]. Theoretical configurations are labeled using the short-hand notation $[p_1(p_2 p_3), (n_1 n_2)n_3]$, where p_1 represents the number of $\pi h_{11/2}$ protons and n_3 the number of $\nu i_{13/2}$ neutrons. The other labels, in parentheses, are only used if nonzero: p_2 and p_3 represent the number of protons of $f_{7/2}/h_{9/2}$ and $i_{13/2}$ character, respectively, while n_1 and n_2 represent the number of neutron holes of $N_{\mathrm{osc}} = 4$ and $h_{11/2}$ character, respectively. The configurations may be written in full as

$$\pi\{(h_{11/2})^{p_1}(f_{7/2}/h_{9/2})^{p_2}(i_{13/2})^{p_3}\} \otimes \tag{6}$$
$$\nu\{(N_{\mathrm{osc}} = 4)^{-n_1}(h_{11/2})^{-n_2}(i_{13/2})^{n_3}\}.$$

The general features of the yrast states in ^{155}Ho are very similar to those of ^{156}Er, where potential energy surfaces were presented in Ref. [41]. For ^{155}Ho, the calculated energies of low-lying states for different types of configuration are shown in Fig. 9, relative to a rotating liquid-drop energy [9]. This figure demonstrates that, for spin values $I \approx 30 - 45$, the lowest-energy configurations are nearly always found at the non-collective oblate shape with $\gamma = 60°$. The corresponding configurations are built from the nine valence particles outside the ^{146}Gd core, or include one-proton particle-hole excitations across $Z = 64$. At higher spins, strongly deformed triaxial (TSD) configurations, involving neutron particle-hole excitations across $N = 82$, come into play. Although no evidence for these collective structures has been found in ^{155}Ho, such bands have been identified in ^{157}Ho from the current experiment [42].
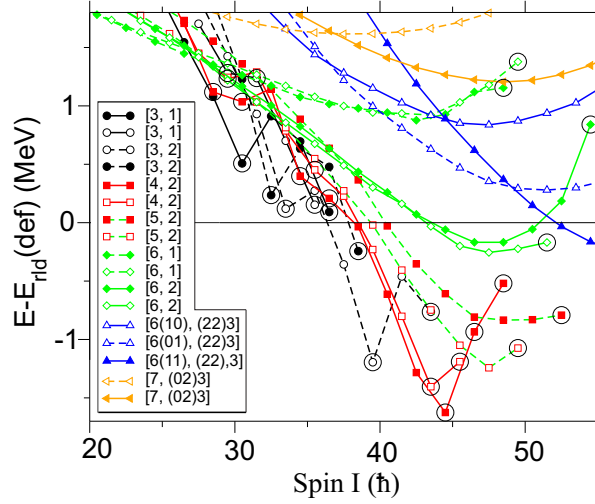
FIG. 9: (Color online) Calculated energies for a selection of fixed configurations in the yrast region of ^{155}Ho, drawn relative to a rotating liquid-drop energy. Different colors and symbols are used for low-lying bands of small collectivity, for bands showing favored terminations, and for more deformed bands at axial and non-axial shapes, respectively. Non-collective oblate states are encircled.

1. Negative-parity states

The bands observed in ^{155}Ho above $I \approx 30$ have been assigned CNS configurations. Their energies are, in general, rather irregular with a down-sloping trend when drawn relative to the rotating liquid-drop reference. Such down-sloping trends are generally calculated in configurations with a closed or almost closed $Z = 64$ proton core, see Fig. 9. Thus, it appears that these bands should be interpreted in terms of the bands in Fig. 9 with at most two holes in the proton core; i.e., with bands having at most five $h_{11/2}$ protons. Considering first negative parity, bands 2 and 6 are compared with the [5,2] and [3,2] configurations in Fig. 10. The terminating state in the favored [3,2] configuration with maximum spin $I_{\mathrm{max}} = 79/2$ can be written as

$$\pi\{(h_{11/2})^3_{27/2}\}_{27/2^-} \otimes \tag{7}$$
$$\nu\{(f_{7/2}/h_{9/2})^4_{14}(i_{13/2})^2_{12}\}_{26^+}.$$

The proton and neutron configurations are shown in Fig. 11. Comparing with experiment, band 6 is observed to $I = 79/2^-$, which suggests that it should be assigned the [3,2] configuration. Indeed, the fact that this state is strongly favored both experimentally and

theoretically and the observation of analogous states in the neighboring $N = 88$ isotones give strong support to this interpretation.
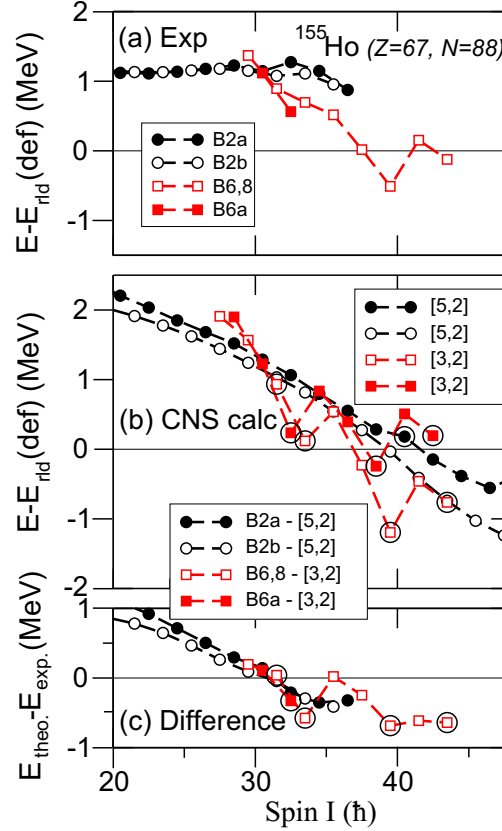

FIG. 10: (Color online) The observed negative-parity high-spin states in ^{155}Ho are shown in (a) relative to the rotating liquid-drop reference, the calculated bands assigned to them are presented in (b), with the difference between calculations and experiment in (c). The calculated bands are labelled by the number of $h_{11/2}$ protons and by the number of $i_{13/2}$ neutrons (see text for further details). Non-collective oblate states are encircled.

The negative-parity states with $I^\pi = 83/2^-$ and $87/2^-$ (structure 8 in Fig. 1) which feed the $I^\pi = 79/2^-$ state are also included in Fig. 10(a). They are well described by the continuation of the [3,2] configuration, where one proton is excited from the $d_{5/2}$ shell below the $Z = 64$ gap to the $d_{3/2}$ one above the gap. Such an excitation will add $5/2 + 3/2 = 4\hbar$ to the $I_{\max}$ value (87/2). Particle-hole excitations of this type are generally predicted relative to closed-core maximum-spin states.

Non-collective states in the [3,2] configuration with one spin vector in the opposite direction to those of the other valence particles can also be formed. If one $m_i = 7/2$ orbital of
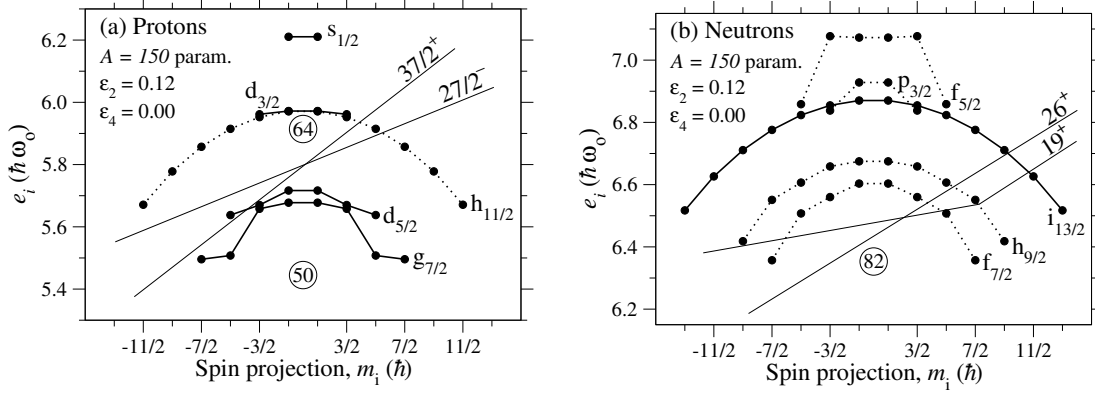
FIG. 11: Tilted Fermi-surface diagrams for (a) protons and (b) neutrons at an oblate shape, showing the configurations of the yrast $I^\pi = 79/2^-$ and $I^\pi = 89/2^+$ terminating states in ^{155}Ho, built from $27/2^-$ and $37/2^+$ proton configurations coupled to a 26^+ neutron configuration. The $I^\pi = 65/2^-$ favored state of band 6 is built from the $27/2^-$ proton configuration coupled to a 19^+ neutron configuration.

$f_{7/2}/h_{9/2}$ character is moved to an $m_i = -7/2$ orbital, a state with $I = 79/2 - 7/2 - 7/2 = 65/2$ is formed. This is analogous to how the $I = 40^+$ or 43^- states are formed in ^{158}Er with one anti-aligned spin vector relative to the fully aligned 46^+ and 49^- states [43]. As seen in Fig. 10, the $65/2^-$ state in band 6a of ^{155}Ho is particularly low in energy and agrees with the calculated $65/2^-$ level. If instead the $m_i = 5/2$ orbital of $f_{7/2}/h_{9/2}$ character is moved to an $m_i = -7/2$ orbital, a low-lying $I = 79/2 - 6 = 67/2$ level is formed as seen for the calculated configurations in Fig. 10(b), but no such state is seen experimentally, see Fig. 10(a). Indeed, the strong transition connecting the $67/2^-$ state of band 6 and the $65/2^-$ suggests that these two states have a similar character but this is not supported by the observed energies, where the $65/2^-$ state is clearly favored, but the $67/2^-$ state follows the smooth trend within the band. However, even if there exists a low-lying aligned $67/2^-$ state, the experimental decay starting from the fully aligned $79/2^-$ might bypass this and follow the smooth trend of the more collective branch.

The strong 638-keV transition which feeds the $65/2^-$ favored state in ^{155}Ho is notable for having a particularly low angular-distribution ratio of 0.51(3). Fitting the angular-distribution function [44] for this γ ray yields an angular-distribution coefficient of $A_2 = -0.68(9)$, which indicates that the $M1/E2$ transition has a large, negative $E2/M1$

multipole mixing ratio, and, hence, significant ($\sim 50\%$) nonstretched-$E2$ admixture. In ^{157}Er there is a $77/2^-$ state which corresponds to the $65/2^-$ state in ^{155}Ho coupled to an extra $m_i = 5/2$, $h_{11/2}$ proton and an extra $m_i = 7/2$, $h_{9/2}$ neutron, see Fig. 9 and Ref. [45]. It too is particularly favored and is also fed by an $M1/E2$ transition with an unusual angular-distribution coefficient of $A_2 = -0.875(15)$, again indicating a large, negative $E2/M1$ multipole mixing ratio and significant nonstretched-$E2$ component [46].

At low spin, band 2 is understood as having the odd particle in the $h_{11/2}$ orbitals, which means that when pairing starts to become less important at high spin it should be assigned to a configuration with an odd number of $h_{11/2}$ particles. Indeed, as seen in Fig. 10, the high-spin range of the band is well described by the [5,2] configuration. Thus, the general features of the differences in the lower panel comes out as expected. The pairing energy will continuously become larger with decreasing spin values as has been verified in explicit calculations on ^{161}Lu [47]. Thus, with pairing included, the differences in Fig. 10 would be close to constant supporting the present assignments. Note also that in this interpretation the high spin range of band 2 is consistent with the band-head interpretation, corresponding to an odd number of $h_{11/2}$ protons and an even number of $i_{13/2}$ neutrons.

It is also interesting that the [5,2] configuration comes close to the continuation of the [3,2] configuration beyond the fully aligned $I = 79/2$ state. The [3,2] states at $I = 83/2, 87/2$ are formed when one particle is excited across the $Z = 64$ gap. As there are several observed negative-parity states at similar energies for these spin values, some of them might be assigned to the [5,2] configuration.

2. Positive-parity states

The positive-parity states observed at high spin belong to bands 5 and 7. The spin values and the parities in band 7 are tentative and partly chosen because there is then a close agreement with the highest-spin states in the valence space of the [4,2] configuration, as seen in Fig. 12. The terminating $I^\pi = 89/2^+$ level is formed from the combination of the $37/2^+$ proton state and the 26^+ neutron one illustrated in Fig. 11 (this figure also shows how the $I^\pi = 79/2^-$ state is formed). The $I^\pi = 87/2^+$ state is then formed with the proton hole in the $m_i = -3/2$ orbital of $d_{5/2}/g_{7/2}$ character. Specifying the occupation of the different
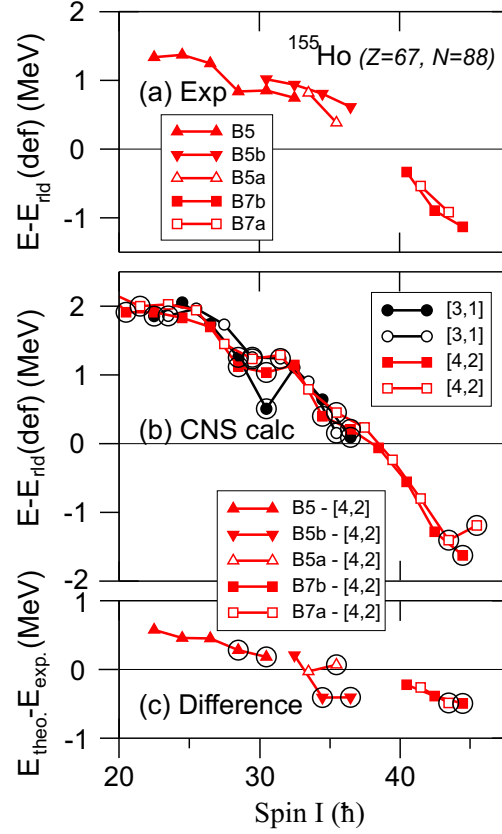
FIG. 12: (Color online) Same as Fig. 10 but for positive parity. Both the caculated [4,2] and [3,1] configurations are shown in the middle panel but only the difference compared with the [4,2] configuration in the lower panel. Thus, for signature $\alpha = +1/2$, the lowest calculated [4,2] states are compared with band 5 for $I = 22.5 - 30.5$, with band 5b for $I = 32.5 - 36.5$, and band 7b for $I = 40.5 - 44.5$.

j-shells and the maximum spin values, these states can be written as

$$\pi(d_{5/2}/g_{7/2})^{-1}_{3/2,5/2,7/2}(h_{11/2})^4_{16} \; \otimes \tag{8}$$
$$\nu(f_{7/2}/h_{9/2})^4_{14}(i_{13/2})^2_{12},$$

where the $91/2^+$ state has also been included, with the proton hole in the $m_i = -7/2$ orbital. As can be understood from Fig. 11, and as seen in Fig. 12(b), this state is calculated at a relatively low energy.

The states in bands 5 and 5b have signature $\alpha = 1/2$ and are rather well described by the [3,1] configuration. Band 5b is observed to an $I^\pi = (73/2^+)$ state, which is the highest spin that can be created with signature $\alpha = 1/2$ in the closed-core [3,1] configuration.

Furthermore, this state is favored in energy both in calculations and experiment, supporting this interpretation. However, one problem is that a low-lying $I = 61/2$ level (with one $f_{7/2}/h_{9/2}$ neutron anti-aligned) is calculated with no experimental counterpart. In addition, the observed band 5b has the same signature as band 5 and is only around 200 keV higher in energy for the two common spin values in the bands, $61/2^+$ and $65/2^+$. Band 5b has many connections with band 5 which suggests that it should also be assigned to a [3,1] configuration. However, it appears difficult to build another such low-lying [3,1] band in the CNS formalism.

An alternative is to assign bands 5 and 5b as [4,2] configurations. As seen in Fig. 12(b), this configuration is calculated at energies similar to the [3,1] ones at the spin values where band 5 is observed, $I \approx 20 - 35$. Thus, it agrees well with the experimental states of band 5 which are drawn in Fig. 12(a).

Some non-collective states with one or two anti-aligned spin vectors are competitive in energy in the [4,2] configuration. Thus, the $h_{11/2}$ protons and the $f_{7/2}/h_{9/2}$ neutrons in the configuration labeled 8 might couple not only to their maximum spin values, $I_{\max} = 16$ and 14, respectively, but also to $I = 8$ and 8 (cf. Fig. 11). Therefore, bands which terminate at $I^\pi = 61/2^+$, $73/2^+$ and $77/2^+$ might be formed as supported by the aligned yrast states with $I = 30.5, 36.5$ drawn in Fig. 12(b), while it appears that the aligned 38.5 state is not yrast. The observed bands give some support to this assumption, because the lowest $61/2^+$ state is fed by four transitions, while $73/2^+$ is the highest observed spin in band 5b. The presence of bands terminating at different spin values gives a natural explanation of the two close-lying $61/2^+$ and $65/2^+$ states. No connection between band 5 and 7 was observed experimentally which may appear strange as they have the same [4,2] configuration. However, if the $73/2^+$ state in band 5 is non-collective then this would be expected. Considering these different features, it appears that the [4,2] configuration is the most likely interpreaton of bands 5 and 5a. Therefore, the difference compared with this configuration is plotted in Fig. 12(c), where also the difference between the two states in band 5a and the $\alpha = -1/2$ signature of the [4,2] configuration are shown.
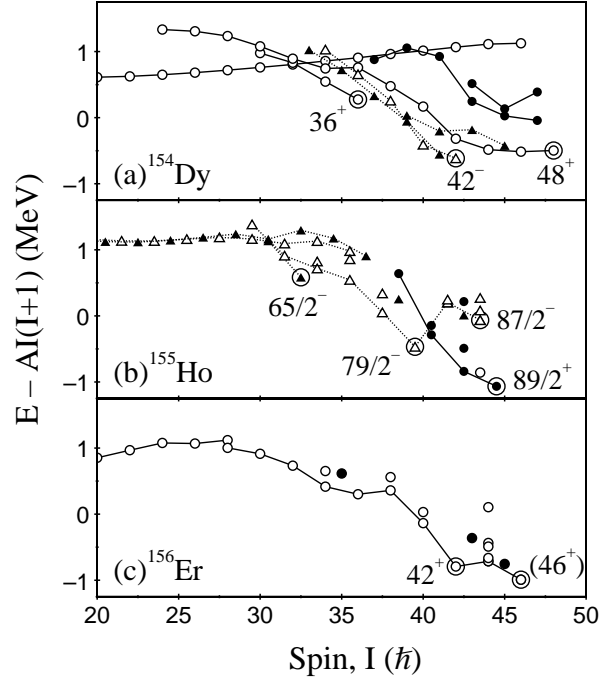
FIG. 13: Experimental energies plotted relative to a rigid-rotation reference. The constant A is 0.00731, 0.00723, and 0.00715 MeV/$\hbar^2$ [9] for (a)^{154}Dy, (b)^{155}Ho, and (c)^{156}Er, respectively. Non-collective oblate states are encircled.

3. Comparison with neighboring $N = 88$ isotones

In order to trace the terminating states across a range of $N = 88$ isotones, the energies relative to a rotating reference of the highest-spin, negative-parity $^{155}_{67}$Ho states are plotted in Fig. 13 alongside levels in $^{154}_{66}$Dy [48, 49] and $^{156}_{68}$Er [4, 41]. The 79/2$^-$ terminating state in ^{155}Ho can be identified in ^{156}Er and ^{154}Dy with the addition or removal of the least favored protons. For instance, the favored positive-parity terminating state in ^{156}Er at $I^\pi = 42^+$ represents the addition of an extra proton in the $m_i = 5/2$ orbital of the $h_{11/2}$ subshell. Similarly, the 36$^+$ level in ^{154}Dy represents the 79/2$^-$ ^{155}Ho configuration with one less $m_i = 7/2$ $h_{11/2}$ proton. These configurations are easy to understand from Fig. 11. They are given in full, relative to the doubly magic ^{146}Gd core, in Table VI. A terminating state in ^{157}Ho [50] is also listed in the table. A detailed discussion of the systematics of even-even $N = 88$ isotones ($Z = 64$ to 70) at high spin can be found in Ref. [41].

TABLE VI: Observed non-collective oblate states in ^{155}Ho and neighboring nuclei.

Nucleus	I^π	Configuration		
$Z = 67$ isotopes				
^{155}Ho	$65/2^-$	$\pi\{(h_{11/2})^3_{27/2}\}_{27/2^-}$	$\otimes$	$\nu\{(i_{13/2})^2_{12}(f_{7/2}/h_{9/2})^4_7\}_{19^+}$
^{155}Ho	$79/2^-$	$\pi\{(h_{11/2})^3_{27/2}\}_{27/2^-}$	$\otimes$	$\nu\{(i_{13/2})^2_{12}(f_{7/2}/h_{9/2})^4_{14}\}_{26^+}$
^{155}Ho	$87/2^-$	$\pi\{(d_{5/2}/g_{7/2})^{-1}_{5/2}(h_{11/2})^3_{27/2}(d_{3/2})^1_{3/2}\}_{35/2^-}$	$\otimes$	$\nu\{(i_{13/2})^2_{12}(f_{7/2}/h_{9/2})^4_{14}\}_{26^+}$
^{155}Ho	$87/2^+$	$\pi\{(d_{5/2}/g_{7/2})^{-1}_{3/2}(h_{11/2})^4_{16}\}_{35/2^+}$	$\otimes$	$\nu\{(i_{13/2})^2_{12}(f_{7/2}/h_{9/2})^4_{14}\}_{26^+}$
^{155}Ho	$89/2^+$	$\pi\{(d_{5/2}/g_{7/2})^{-1}_{5/2}(h_{11/2})^4_{16}\}_{37/2^+}$	$\otimes$	$\nu\{(i_{13/2})^2_{12}(f_{7/2}/h_{9/2})^4_{14}\}_{26^+}$
^{157}Ho	$87/2^-$	$\pi\{(h_{11/2})^3_{27/2}\}_{27/2^-}$	$\otimes$	$\nu\{(i_{13/2})^2_{12}(f_{7/2}/h_{9/2})^6_{18}\}_{30^+}$
$N = 88$ isotones				
^{154}Dy	36^+	$\pi\{(h_{11/2})^2_{10}\}_{10^+}$	$\otimes$	$\nu\{(i_{13/2})^2_{12}(f_{7/2}/h_{9/2})^4_{14}\}_{26^+}$
^{154}Dy	42^-	$\pi\{(d_{5/2}/g_{7/2})^{-1}_{5/2}(h_{11/2})^3_{27/2}\}_{16^-}$	$\otimes$	$\nu\{(i_{13/2})^2_{12}(f_{7/2}/h_{9/2})^4_{14}\}_{26^+}$
^{154}Dy	48^+	$\pi\{(d_{5/2}/g_{7/2})^{-2}_6(h_{11/2})^4_{16}\}_{22^-}$	$\otimes$	$\nu\{(i_{13/2})^2_{12}(f_{7/2}/h_{9/2})^4_{14}\}_{26^+}$
^{156}Er	42^+	$\pi\{(h_{11/2})^4_{16}\}_{16^+}$	$\otimes$	$\nu\{(i_{13/2})^2_{12}(f_{7/2}/h_{9/2})^4_{14}\}_{26^+}$
^{156}Er	46^+	$\pi\{(d_{5/2}/g_{7/2})^{-1}_{5/2}(h_{11/2})^4_{16}(d_{3/2})^1_{3/2}\}_{20^+}$	$\otimes$	$\nu\{(i_{13/2})^2_{12}(f_{7/2}/h_{9/2})^4_{14}\}_{26^+}$

4. Band termination in ^{156}Er

Figure 13(c) includes the (46^+) state in ^{156}Er. This level appears to be very favored, and it is proposed that it is the 46^+ state which is predicted to be energetically favored in CNS calculations [41]. While the $I = 42^+$ state represents the maximum spin achievable involving the six valence neutrons and four valence protons outside the ^{146}Gd core, the 46^+ configuration involves a proton being excited across the $Z = 64$ shell gap from the $\pi d_{5/2}/g_{7/2}$ subshell into the $d_{3/2}$ one. This is analogous to the formation of the $87/2^-$ state in ^{155}Ho on top of the $79/2^-$ state. The full configurations are given in Table VI.

V.   CONCLUSIONS

A high-statistics, high-spin experiment has been performed to study the level structure of ^{155}Ho. Many previously unreported γ-ray transitions have been established and a comprehensive level scheme has been built from high-fold coincidence analysis. At low spin, a positive-parity $\pi g_{7/2}$ rotational band, observed for the first time in this nucleus, has been established up to $(33/2^+)$. The more favored $\pi h_{11/2}$ band has been extended to $I^\pi = (73/2^-)$. A positive-parity rotational structure has been established to $I^\pi = 57/2^+$ and interpreted as being based on a $\nu(i_{13/2}h_{9/2})$ structure coupled to the $h_{11/2}$ proton. $B(M1)/B(E2)$ ratios of reduced transition probabilities have been calculated from observed branching ratios for all three bands and compared with geometric model calculations for specific particle configurations. While these are mostly in agreement, the $B(M1)/B(E2)$ ratios measured for the $\pi(h_{11/2}) \otimes \nu(i_{13/2}h_{9/2})$ band exhibit a striking signature dependence, which cannot be fully explained by the observed energy-splitting between the $\alpha = +1/2$ and $\alpha = -1/2$ signature components.

The $\pi h_{11/2}$ configuration has been discussed as favoring a negative γ triaxial deformation, which gives rise to the considerable signature splitting in the band up to spin ~ 15, at which point it is quenched by the $(\nu i_{13/2})^2$ alignment. This effect is common to the $\pi h_{11/2}$ bands of other nuclei in this region.

Above spin $\sim 30\hbar$, terminating bands in ^{155}Ho have been seen. Several energetically favored terminating states built on specific particle configurations were identified, including a state at $I^\pi = 79/2^-$, which corresponds to valence-space band termination in ^{155}Ho. States of higher spin and excitation energy are thought to correspond to predicted favored states at oblate deformation, with $I^\pi = 87/2^-$ and $89/2^+$. These states are built on $\pi(d_{5/2}/g_{7/2} \rightarrow d_{3/2})$ and $\pi(d_{5/2}/g_{7/2} \rightarrow h_{11/2})$ particle-hole excitations, respectively, across the $Z = 64$ shell gap.

[1] T. Bengtsson and I. Ragnarsson, Phys. Scr. **T5**, 165 (1983).

[2] C. Baktash *et al.*, Phys. Rev. Lett. **54**, 978 (1985).

[3] I. Ragnarsson, T. Bengtsson, W. Nazarewicz, J. Dudek, and G. A. Leander, Phys. Rev. Lett. **54**, 982 (1985).

[4] F. S. Stephens, M. A. Deleplanque, R. M. Diamond, A. O. Macchiavelli, and J. E. Draper, Phys. Rev. Lett. **54**, 2584 (1985).

[5] I. Ragnarsson and T. Bengtsson, Nucl. Phys. **A447**, 251c (1985).

[6] J. Dudek and W. Nazarewicz, Phys. Rev. C **31**, 298 (1985).

[7] I. Ragnarsson, Z. Xing, T. Bengtsson, and M. A. Riley, Phys. Scr. **34**, 651 (1986).

[8] A. O. Evans *et al.*, Phys. Rev. Lett. **92**, 252502 (2004).

[9] A. V. Afanasjev, D. B. Fossan, G. J. Lane, and I. Ragnarsson, Phys. Rep. **322**, 1 (1999).

[10] T. Bengtsson and I. Ragnarsson, Nucl. Phys. A **436**, 14 (1985).

[11] B. G. Carlsson and I. Ragnarsson, Phys. Rev. C **74**, 011302(R) (2006).

[12] J. M. Rees, Ph. D. Thesis, University of Liverpool (2013).

[13] J. M. Rees *et al.*, Phys. Rev. C **83**, 044314 (2011).

[14] X. Wang *et al.*, Phys. Lett. B **702**, 127 (2011).

[15] I. Y. Lee, Nucl. Phys. A **520**, 641c (1990).

[16] R. V. F. Janssens and F. S. Stephens, Nucl. Phys. News **6**, 9 (1996).

[17] D. C. Radford, Nucl. Instrum. and Methods Phys. Res. A **361**, 297 (1995).

[18] D. C. Radford, M. Cromaz, and C. J. Beyer, in *Proceedings of the Nuclear Structure '98 Conference, Gatlinburg, 1998*, edited by C. Baktash (American Institute of Physics CP481, 1999), p. 570.

[19] K. S. Krane, R. M. Steffen, and R. M. Wheeler, Nucl. Data Tables A **11**, 351 (1973).

[20] C. W. Beausang *et al.*, Nucl. Instrum. Methods Phys. Res. A **364**, 560 (1995).

[21] C. W. Reich, Nucl. Data Sheets **104**, 1 (2005), and references therein.

[22] C. Foin, S. Andre, D. Barneoud, J. Boutet, G. Bastin, M. G. Desthuilliers, and J. P. Thibaud, Nucl. Phys. A **324**, 182 (1979).

[23] H. Helppi, D. C. Radford, R. Holtzmann, R. V. F. Janssens, T. L. Khoo, R. Broda, P. J. Daly, and Z. Grabowski, in *Proceedings of the International Nuclear Physics Conference, Harrogate, 1986*, edited by J. L. Durell, J. M. Irvine, and G. C. Morrison (Institute of Physics Conference Series Number 86, 1986) p. 115.

[24] I. Ragnarsson, A. Sobiczewski, R. K. Sheline, S. E. Larsson, and B. Nerlo-Pomorska, Nucl. Phys. A **233**, 329 (1974).

[25] R. F. Casten, D. D. Warner, D. S. Brenner, and R. L. Gill, Phys. Rev. Lett. **47**, 1433 (1981).

[26] R. Bengtsson and S. Frauendorf, Nucl. Phys. A **327**, 139 (1979).

[27] S. M. Harris, Phys. Rev. **138**, B509 (1965).

[28] J. Simpson *et al.*, J. Phys. G **12**, L67 (1986).

[29] F. Dönau and S. Frauendorf, in *Proceedings of the Conference on High Angular Momentum Properties of Nuclei, Oak Ridge, Tenn., 1982*, edited by N. R. Johnson (Harwood Academic, New York, 1983), p. 143.

[30] F. Dönau, Nucl. Phys. A **471**, 469 (1987).

[31] J. P. Torres, P. Paris, D. Lecouturier, and P. Kilcher, Nucl. Phys. A **189**, 609 (1972).

[32] J. Simpson *et al.*, Phys. Rev. Lett. **54**, 1132 (1985).

[33] A. J. Kreiner, M. A. J. Mariscotti, C. Baktash, E. der Mateosian, and P. Thieberger, Phys. Rev. C **23**, 748 (1981).

[34] S. Frauendorf and F. R. May, Phys. Lett. B **125**, 245 (1983).

[35] G. B. Hagemann, J. D. Garrett, B. Herskind, J. Kownacki, B. M. Nyako, P. L. Nolan, J. F. Sharpey-Schafer, and P. O. Tjom, Nucl. Phys. A **424**, 365 (1984).

[36] E. S. Paul *et al.*, Phys. Rev. C **80**, 054312 (2009).

[37] G. B. Hagemann and I. Hamamoto, Phys. Rev. C **40**, 2862 (1989).

[38] T. Bengtsson, Nucl. Phys. A **512**, 124 (1990).

[39] K. Pomorski and J. Dudek, Phys. Rev. C **67**, 044316 (2003).

[40] K. T. R. Davies and J. R. Nix, Phys. Rev. C **14**, 1977 (1976).

[41] E. S. Paul *et al.*, Phys. Rev. C **79**, 044324 (2009).

[42] X. Wang *et al.*, J. Phys. Conf. Series **381**, 012065 (2012).

[43] J. Simpson *et al.*, Phys. Lett. B **327**, 187 (1994).

[44] T. Yamazaki, Nucl. Data A **3**, 1 (1967).

[45] S. J. Gale *et al.*, J. Phys. G **21**, 193 (1995).

[46] A. O. Evans *et al.*, Phys. Rev. C **73**, 064303 (2006).

[47] H.-L. Ma, B. G. Carlsson, I. Ragnarsson, and H. Ryde, Phys. Rev. C **90**, 014316 (2014).

[48] H. W. Cranmer-Gordon *et al.*, Nucl. Phys. A **465**, 506 (1987).

[49] W. C. Ma *et al.*, Phys. Rev. C **65**, 034312 (2002).

[50] D. C. Radford *et al.*, Nucl. Phys. A **545**, 665 (1992).